2014

PRC2 is recurrently inactivated through EED or SUZ12 loss in malignant peripheral nerve sheath tumors

W. Lee

S. Teckie
Hofstra Northwell School of Medicine

T. Wiesner

A. Viale

S. Singer

See next page for additional authors

HHS Public Access

Author manuscript

Nat Genet. Author manuscript; available in PMC 2015 May 01.

Published in final edited form as:

Nat Genet. 2014 November ; 46(11): 1227–1232. doi:10.1038/ng.3095.

PRC2 is recurrently inactivated through *EED* or *SUZ12* loss in malignant peripheral nerve sheath tumors

William Lee[1,3,17], **Sewit Teckie**[2,3,17], **Thomas Wiesner**[2,17], **Leili Ran**[2,17], **Carlos N. Prieto Granada**[4], **Mingyan Lin**[5], **Sinan Zhu**[2], **Zhen Cao**[2], **Yupu Liang**[2], **Andrea Sboner**[6,7,8], **William D. Tap**[9], **Jonathan A. Fletcher**[10], **Kety H. Huberman**[12], **Li-Xuan Qin**[11], **Agnes Viale**[12], **Samuel Singer**[13], **Deyou Zheng**[5,14,15], **Michael F. Berger**[2,4], **Yu Chen**[2,9,16], **Cristina R. Antonescu**[4], and **Ping Chi**[2,9,16]

[1]Computational Biology Program, Memorial Sloan-Kettering Cancer Center, 1275 York Avenue, New York, NY 10065

[2]Human Oncology and Pathogenesis Program, Memorial Sloan-Kettering Cancer Center, 1275 York Avenue, New York, NY 10065

[3]Department of Radiation Oncology, Memorial Sloan-Kettering Cancer Center, 1275 York Avenue, New York, NY 10065

[4]Department of Pathology, Memorial Sloan-Kettering Cancer Center, 1275 York Avenue, New York, NY 10065

[5]Department of Genetics, Albert Einstein College of Medicine, Bronx, NY 10461

[6]Department of Pathology and Laboratory Medicine, Weill Cornell Medical College/New York Presbyterian Hospital, 1300 York Avenue, New York, NY 10065

[7]Institute for Computational Biomedicine, Weill Cornell Medical College/New York Presbyterian Hospital, 1300 York Avenue, New York, NY 10065

[8]Institute for Precision Medicine, Weill Cornell Medical College/New York Presbyterian Hospital, 1300 York Avenue, New York, NY 10065

[9]Department of Medicine, Memorial Sloan-Kettering Cancer Center, 1275 York Avenue, New York, NY 10065

Corresponding author: Ping Chi, MD, PhD, Memorial Sloan Kettering Cancer Center, 1275 York Avenue, New York, NY 10065, chip@mskcc.org.

[17]These authors contributed equally to this work

AUTHOR CONTRIBUTIONS

Project planning and experimental design: P.C., C.R.A.,Y.C., T.W., W.L., S.T., R.L.; Sample collection and clinical database, cell lines, S. T., S.S., C.R.A., C.N.P.G., J.A.F. W.D.T.; Pathology review: C.R.A., C.N.P.G.; Preparation of DNA, RNA and next-generation sequencing libraries: T.W., S.T., A.V.; Sequence data analysis: W.L., Y.C., S.T., P.C., M.F.B., M.L., D.Z., Y.L., A.S.; Immunohistochemistry (IHC): T.W.; Western blots, Immunofluorescence (IF), growth curves and all cellular assay: L. R., S. Z.; Generation of the expression vectors: Z.C., L.R.; Biostatistics, L.Q.; Manuscript writing: P.C., Y.C., W.L., T.W., L.R.; Review of the final manuscript: all authors.

COMPETING FINANCIAL INTERESTS

The authors declare no competing financial interests.

[10]Department of Pathology, Brigham and Women's Hospital, 75 Francis Street, Boston, MA 02115

[11]Department of Epidemiology and Biostatistics, Memorial Sloan-Kettering Cancer Center,1275 York Avenue, New York, NY 10065

[12]Genomics Core Laboratory, Memorial Sloan-Kettering Cancer Center, 1275 York Avenue, New York, NY 10065

[13]Department of Surgery, Memorial Sloan-Kettering Cancer Center, 1275 York Avenue, New York, NY 10065

[14]Department of Neurology, Albert Einstein College of Medicine, Bronx, NY 10461

[15]Department of Neuroscience, Albert Einstein College of Medicine, Bronx, NY 10461

[16]Department of Medicine, Weill Cornell Medical College, 130 York Avenue, New York, NY

Abstract

Malignant Peripheral Nerve Sheath Tumors (MPNSTs) represent a group of highly aggressive soft tissue sarcomas that may occur sporadically, in association with neurofibromatosis type I (NF1-), or after radiotherapy[1–3]. Using comprehensive genomic approaches, we identified loss-of-function (LOF) somatic alterations of the Polycomb repressive complex 2 (PRC2) core components, *EED* or *SUZ12*, in 92% of sporadic, 70% of NF1-associated and 90% of radiotherapy-associated MPNSTs. MPNSTs with PRC2 loss showed complete loss of H3K27me3 and aberrant transcriptional activation of multiple PRC2-repressed homeobox master regulators and their regulated developmental pathways. Introduction of the PRC2 component in a PRC2-deficient MPNST cell line restored H3K27me3 and decreased cell growth. Additionally, we identified frequent somatic alterations of *CDKN2A* (81% of all MPNSTs) and *NF1* (72% of non-NF1-associated MPNSTs), and they significantly co-occur with PRC2 alterations. The highly recurrent and specific inactivation of PRC2, *NF1*, *CDKN2A* posits their critical and potentially cooperative roles in MPNST pathogenesis.

MPNSTs arise from peripheral nerves and associated cellular components and represent a highly aggressive subtype of soft tissue sarcoma[1]. MPNSTs metastasize early and are often resistant to radiotherapy and chemotherapy. Conventional MPNSTs present in three distinct clinical settings: sporadically, in association with neurofibromatosis type I (NF1-associated) or prior radiotherapy (radiotherapy-associated), respectively accounting for approximately 45%, 45% and 10% of cases[2,5]. Histologically, MPNSTs are characterized by intersecting fascicles of monotonous spindle cells with hyperchromatic nuclei and high mitotic counts with focal areas of necrosis, but accurate diagnosis remains challenging due to the lack of specific immunohistochemical (IHC) and molecular biomarkers[5,6]. Among NF1-patients, loss of the non-mutant allele is thought to be the key driver in benign NF1-associated neurofibromas[7]. Little is known of the genetic alterations that mediate progression from neurofibromas into MPNST in NF1-patients or of the molecular pathogenesis of sporadic and radiotherapy-associated MPNSTs.

To investigate the molecular basis of MPNSTs, we performed whole-exome sequencing (WES), DNA copy-number and loss-of-heterozygosity (LOH) profiling and whole-transcriptome sequencing (RNA-seq) of a discovery cohort consisting of normal-tumor paired tissues of 15 MPNSTs from 12 patients (6 NF1-associated, 4 sporadic, 4 radiotherapy-associated and 1 epithelioid MPNSTs) (Supplementary Table 1, 2). Epithelioid MPNST is a rare histological variant of MPNST, composed of exclusively epithelioid malignant cells with diffuse immunoreactivity for the S100 protein, and is not associated with NF1[6].

We identified 4 frame-shift and 1 splice-site mutations in *EED* (Fig. 1a, c and Supplementary Fig. 1). RNA-seq validated aberrant *EED* splicing in the splice-site mutated sample (Supplementary Fig. 2a). All five samples showed LOH of the *EED* locus, three samples (11T, 12T, 14T) by heterozygous deletion of the normal allele (Supplementary Fig. 1b) and two samples (15T, 16T) by copy-neutral LOH (Supplementary Fig. 2b). This data suggests that samples with *EED* mutation have complete loss of EED function.

We further identified 2 homozygous (Hom deletion) and 5 heterozygous (Het loss) deletions of *SUZ12* (Fig. 1a, c and Supplementary Fig. 1 and 3a). We examined RNA-seq profiles of the *SUZ12* transcript among the 5 Het loss samples. Two samples, 9T and 12T (with *EED H213fs*) expressed full-length *SUZ12* transcript (Supplementary Fig. 1b, not shown). Remarkably, the other 3 samples display structural alterations of *SUZ12* transcript, starting at exon 6, exon 10 and exon 4 in 2T, 7T and 13T, respectively (Supplementary Fig. 3b–d). These are likely due to local genomic rearrangements of the remaining copy, which were not identified by standard WES analysis. Indeed, for 7T and 18T, derived from two tumors from the same patient, there is a DNA break in exon 10 upon manual examination of WES data (Supplementary Fig. 3c). We designated these cases as structural variation (SV) and Het loss at the *SUZ12* locus, and intriguingly they all occurred in radiotherapy-associated MPNSTs (Fig. 1a).

EED and SUZ12 are the core components of PRC2, and together with EZH1/EZH2, establish and maintain the di- and tri-methylation of Lys27 of histone H3 (H3K27me2/3)[8]. *EED* and *SUZ12* genetic alterations are mutually exclusive and are collectively found in 80% (12/15) of all MPNSTs (Fig. 1a, c). We did not observe any genetic alterations in other PRC2 core members including *EZH1* and *EZH2* (Supplementary Table 3).

We found recurrent nonsense mutations and Hom deletion in *NF1* in 87.5% (7/8) of sporadic and radiotherapy-associated MPNSTs (Fig. 1a and Supplementary Fig. 1). This data combined with the germline mutations in *NF1* in NF1-associated MPNSTs suggest that NF1 is a uniquely important tumor suppressor in MPNSTs. Alterations of the *CDKN2A* locus and of *TP53* have been reported in MPNSTs[9–12]. We observed Hom deletion and Het loss of the *CDKN2A* locus in 73% (11/15) and 13% (2/15) of MPNSTs, respectively. We also observed non-synonymous mutations and Het loss in *TP53* in 13% (2/15) and 20% (3/15) of MPNSTs. We did not identify other recurrent somatic alterations with relatively high frequency (Supplementary Table 3).

Next, we used a targeted sequencing approach (IMPACT[13], Supplementary Table 4) to characterize a validation cohort of formalin-fixed paraffin-embedded (FFPE) samples consisting of 37 MPNSTs and 7 neurofibromas from 32 patients (Fig. 1b and Supplementary Table 1). Combining the discovery and validation cohorts, we observed PRC2 mutations in 70% (19/27) of NF1-associated, 92% (12/13) of sporadic and 90% (8/9) of radiotherapy-associated MPNSTs (Fig. 1a–d). Genetic alterations in *NF1* were identified in 82% (18/22) of sporadic and radiotherapy-associated MPNSTs. Genetic alterations in *CDKN2A* and *TP53* were found in 81% (42/52) and 42% (22/52) of all MPNSTs respectively (Fig. 1a,b). There is a significant co-occurrence of *NF1*, *CDKN2A* and PRC2 genetic alterations (Fleiss' Kappa statistics, Kappa=0.21, $p=0.001$)[14], suggesting that these are three critical pathways in pathogenesis of conventional MPNSTs. In the 7 NF1-associated neurofibromas, we observed few PRC2 and *CDKN2A* alterations suggesting they may be associated with malignant progression to MPNST. None of the three epithelioid MPNSTs had genetic alterations in the three critical pathways, suggesting that they represent a distinct entity.

To understand the effect of PRC2 loss, we performed gene expression analysis in 16 MPNSTs (Supplementary Table 1). Principal component analysis (PCA) showed all samples with *EED* mutations or *SUZ12* Hom deletion clustered together, and separated from the others by the first principal component (PC1) (Fig. 1a and 2a). Among the five samples with Het loss of *SUZ12*, three with SV (2T, 7T, 13T) and one with *EED H213fs* (12T) clustered among the PRC2-loss group and one with intact transcript (9T) clustered with the PRC2 wild-type group. These observations highlight the complexity of identifying structural variations to accurately determine the PRC2 status in cases of Het loss.

To explore the transcriptional consequence of PRC2 loss, we generated a gene set of differentially expressed genes between PRC2-loss and PRC2-wt MPNSTs (Supplementary Table 5). Hierarchical clustering of these genes robustly separated the PRC2-loss and PRC2-wt MPNSTs. The vast majority of genes (455/479, 95%) were upregulated in PRC2-loss MPNSTs, consistent with the role of PRC2 in transcriptional repression (Fig. 2b). Gene ontology (GO) analysis revealed that known PRC2 suppressed targets, including homeobox transcription factors and genes associated with development and morphogenesis, are highly enriched in genes upregulated in PRC2-loss MPNSTs (Fig. 2c, Supplementary Table 6). The gene expression of several prototypical PRC2 suppressed genes confirmed this difference (Fig. 2d). Gene Set Enrichment Analysis (GSEA) showed the most significantly enriched gene sets downregulated in PRC2-loss MPNSTs include "PRC2 module" defined by genes bound by PRC2 components in mouse ES cells[15] (Fig. 2e, Supplementary Table 7) and the H3K27me3 target genes in neural precursor cells [16] (Fig. 2f) and in brain tissue[17] (Fig. 2g). These data indicate that loss of function in PRC2 results in activation of developmentally regulated master regulators and imprinted genes (*i.e. IGF2*) that lead to distinct transcriptome changes.

We evaluated H3K27me3 levels by IHC in FFPE samples of MPNSTs and neurofibromas. While PRC2-wt MPNSTs showed robust staining of H3K27me3, PRC2-loss MPNSTs showed complete loss of H3K27me3 in tumor cells and preservation of the H3K27me3 staining in stromal cells (Fig. 3a). The positive and negative immunostaining for H3K27me3 are highly concordant with the PRC2 wt and homozygous loss genetic status, respectively

(Fig 3b). However Het loss of PRC2 genetic status was not predictive of H3K27me3 IHC staining (Fig. 3b). Among the Het loss samples with associated RNA-seq data, the transcriptional clustering matched the H3K27me3 IHC. This suggests that DNA sequencing (exome or IMPACT) alone cannot predict PRC2 functional status in all MPNSTs and that the H3K27me3 IHC may be more accurate.

All neurofibromas (7/7), which are PRC2 wt except for one sample with *SUZ12* Het loss, retained H3K27me3 immunostaining (Fig. 1b, 3c and 3d). In specimens that contained the interface of MPNST arising from pre-existing benign plexiform neurofibromas, we observed transition from robust H3K27me3 staining in the plexiform neurofibroma to a clear loss in MPNST. These data suggest that PRC2 loss is involved in the malignant progression of benign plexiform neurofibroma into MPNST. Indeed, 56% (19/34) of the NF1-associated MPNSTs have lost H3K27me3 (Fig. 3d). Curiously, a significantly greater percentage (>90%) of sporadic and radiotherapy-associated MPNSTs have lost H3K27me3 staining (Fig. 3d), suggesting that the progression of disease and sequence of genetic inactivation of *NF1*, *CDKN2A* and PRC2 may be different in MPNST that arise in different clinical settings. Unlike NF1-associated MPNSTs that universally arise from pre-existing neurofibromas, sporadic and radiotherapy-associated MPNSTs rarely have identifiable pre-existing benign nerve sheath tumors. In one of the sporadic MPNST sample (16T), the presence of both *NF1* (D1237_splice mutation) and *EED* (E249fs) non-synonymous mutations allowed us to use their prevalence to infer the sequence of genetic events[18]. The largest subpopulation of cells (84%) contains the *NF1* mutation whereas a smaller subpopulation (57%) contains the *EED* mutation, suggesting that the *NF1* mutation occurred first during progression of this sporadic MPNST (Supplementary Fig. 4). The sequence of NF1, PRC2 and CDKN2A inactivation described here are largely correlation, the precise account requires experimental validation with sequential inactivation of each pathway in cell line and mouse models.

To determine whether PRC2 loss is required for MPNST oncogenesis, we screened available human MPNST cell lines using H3K27me3 immunoblot. We identified one MPNST cell line, ST88-14 derived from an NF1-associated MPNST that has lost H3K27me3. RNA-seq identified that ST88-14 has lost expression of SUZ12, and immunoblot confirmed the loss of the SUZ12 protein (Fig. 4a, b, Supplementary Fig. 5). We next introduced Flag-HA-tagged wild type SUZ12 (FH-SUZ12) or EED (FH-EED) into the ST88-14 cell line and into a PRC2-wt MPNST cell line (MPNST724) that maintained H3K27me3 levels (Fig. 4a, b). Only the FH-SUZ12, but not FH-EED, restored the H3K27me3 level in ST88-14 cells and significantly decreased cell growth (Fig. 4a–c). In MPNST724 cells, there was a mild increase of H3K27me3 levels with the introduction of either FH-SUZ12 or FH-EED (Fig. 4a), but neither had any effect on cell growth (Fig. 4c). These data suggest that PRC2 loss contributes to oncogenesis at least in part by promoting cell proliferation and growth in the PRC2-loss MPNSTs.

We next examined the transcriptional and chromatin changes in ST88-14 and MPNST724 cells with introduction of FH-SUZ12, focusing on several known PRC2 regulated genes (*FOXN4*, *IGF2*, *PAX2*, *TLX1*) that are significantly upregulated in PRC2-loss compared to PRC2-wt MPNST patient samples (Fig. 2c). At baseline, ST88-14 cells exhibit increased

expression of *FOXN4, IGF2, PAX2, TLX1* accompanied by loss of PRC2 components (SUZ12 and EZH2), the PRC2-repressive mark, H3K27me3, and reciprocal gain of H3K4me3 and H3K27ac activation marks at their promoters (Fig. 4d and Supplementary Fig. 6). After introduction of FH-SUZ12 in ST88-14 cells, FH-SUZ12 localized to the promoters of these genes. This was accompanied by increased levels of EZH2, H3K27me3 and decreased levels of H3K4me3 and H3K27ac at the promoter regions, as well as decreased transcript levels of these PRC2 target genes. These data suggest that the PRC2 loss has direct impact on transcriptional regulation and introduction of the missing PRC2 component has the ability to at least partially restore PRC2 function.

MPNSTs often exhibit divergent differentiation including rhabdomyoblasts, glandular, squamous and neuroendocrine elements[6]. Our study revealed a high frequency of LOF genetic alterations in *NF1*, *CDKN2A* and PRC2 (*EED* or *SUZ12*), demonstrating that MPNSTs share common molecular pathogenic pathways despite clinical and histological diversity. PRC2 loss activates multiple developmentally suppressed pathways, which may explain the frequent observation of divergent differentiation in MPNSTs. The high frequency of PRC2 loss suggests that the PRC2 mutational status and more accurately H3K27me3 IHC can be used as biomarkers for more acute diagnosis of MPNSTs.

PRC2 was initially thought to be oncogenic: PRC2 components have higher expression in dividing cells and are important to maintain stemness. *EZH2* is overexpressed in a variety of cancers[19,20], and activating *EZH2* mutations are found in a subset of lymphomas[21]. Paradoxically, recent work suggests that PRC2 can be tumor suppressive in distinct contexts with LOF genetic alterations found in up to 25% in myeloid disorders and T-cell acute lymphoblastic leukemia[22–24] and 42% in early T-cell ALL[25]. Notably the majority of LOF alterations are found in *EZH2*[22–25]. Cellular studies and mouse models show that *Ezh1* can maintain suppression of Polycomb genes in the setting of *Ezh2* loss and combined *Ezh1/Ezh2* or *Eed* or *Suz12* loss derepress Polycomb genes and cause *Cdkn2a* mediated growth arrest[26–29]. These findings suggest that MPNST is unique in that complete loss of PRC2 function is important for tumorigenesis and loss of *CDKN2A* may be a critical cooperative event in addition to *NF1* loss.

Data access

Exome sequencing, RNA sequencing, and DNA copy number data are deposited in dbGaP under accession phsXXXXX.

URLs

GENE-E, https://www.broadinstitute.org/cancer/software/GENE-E; Picard, http://picard.sourceforge.net; Aroma.affymetrix, http://aroma-project.org/

METHODS

Human tumor tissue collection

Patient selection and consent protocols are described in the Supplementary Note. Sample annotation is shown in Supplementary Table 1.

For the discovery cohort, the goal was to obtain normal DNA and tumor DNA for WES and SNP 6.0 array and to obtain tumor RNA for RNA-seq. A total of 15 fresh-frozen paired MPNST tumor-normal samples were identified. Tumor and adjacent normal tissue specimens were embedded in optimal cutting temperature (OCT) medium and a histologic section was obtained for review. Cryomolds of both tumor and normal tissues were macrodissected to minimize contamination prior to RNA and DNA preparation. Sample processing was designed to secure samples and minimize identifying information. Specimens with insufficient tissue amount or severely degraded nucleic acids were excluded.

The IMPACT assay is a hybridization capture, next-generation sequencing platform amenable for both fresh frozen DNA and FFPE DNA for targeted sequencing. The panel includes *NF1*, *SUZ12*, *EED*, and *CDKN2A* and TP53[13]. We validated the somatic mutational findings from the discovery cohort by performing IMPACT assay on the same DNA isolated from tumor tissue. In addition, we performed IMPACT assay on FFPE derived DNA from a second cohort of 37 MPNST and 7 neurofibromas from NF1 patients who were diagnosed with concurrent MPNST (see Supplementary Table 1).

Sample preparation and quality control

RNA was extracted from tumor and normal tissues using a modification of the DNA/RNA AllPrep kit (Qiagen). DNA from fresh-frozen tissues was extracted from tumor and normal tissue specimens using the DNeasy blood and tissue kit (Qiagen). DNA from FFPE samples was isolated using QIAamp DNA FFPE Tissue Kit (Qiagen). Each specimen was initially quantified using the NanoDrop UV spectrophotometer and further quantified with the Bioanalyzer assay (Agilent Technologies).

RNA sequencing and analysis

The isolated RNA was processed using the TruSeq RNA sample Prep kit (#15026495, Illumina) according to the manufacturers' protocol. Briefly, the RNA was Poly-A selected, reverse transcribed and the obtained cDNA underwent end-repair, A-tailing, ligation of the indexes & adapters, and PCR enrichment. The libraries were sequenced on an Illumina HiSeq-2500 platform with 51bp paired-end reads to obtain a minimum yield of 40 million reads per sample. The sequence data was processed and mapped to the human reference genome (hg19) using STAR v2.3[30]. Gene expression levels were quantified with htseq-count[31] and normalized using DESeq[32]. Variance of expression levels was calculated for all genes across samples and the 75th percentile was determined as a cutoff. Principal component analysis was performed on the set of genes with variance greater than that cutoff. We used ANOVA to define differentially expressed genes between PRC2 loss and wild-type samples. Genes that showed >8-fold difference in expression AND corrected FDR <0.05 (479 genes) were used for clustering and gene ontology analysis. Hierarchical clustering was performed using Pearson correlation within the GENE-E software and heatmaps were displayed using GENE-E. Gene ontology analysis was performed using DAVID to discovery enriched pathways and gene ontologies[33]. Gene set enrichment analysis to discover gene sets enriched among upregulated genes in PRC2 lost samples was performed using JAVA GSEA 2.0 program[34]. The gene sets use were the Broad Molecular Signatures

Database gene sets c2 (curated gene sets), c5 (gene ontology gene sets), c6 (oncogenic signatures), c7 (immunologic signatures) as well as additional sets “PRC2_Module” and “ES_Core”[15], totaling 6,886 gene sets.

DNA sequencing and analysis

Whole exome sequencing of DNA from fresh-frozen tissue used 1000ng (or 500ng in select cases) of DNA from either tumor or normal samples. DNA was subjected to shearing, end repair, phosphorylation and ligation to barcoded sequencing adaptors per manufacturer’s guidelines. The ligated DNA was size-selected for fragments between 200–400bp. These fragments were multiplexed and underwent exonic hybrid capture with the SureSelect V4+UTRs exome bait (Agilent). The captured DNA was sequenced on an Illumina HiSeq-2500 platform with 75bp paired-end reads. Raw sequences were aligned to the human genome reference sequence (hg19) using BWA[35]. Total read count and coverage depth are shown in Supplementary Table 2. Aligned data were further processed by removing duplicates using Picard followed by indel realignment and base quality score recalibration with GATK[36]. Single nucleotide somatic mutations and somatic indels were called by taking the union of calls made by MuTect[37], Strelka[38], and VarScan and applying a set of heuristic filters as described in the VarScan 2 paper[39]. Mutations were further filtered to remove variants that are present in dbSNP 137 but not in COSMIC v64[40]. The data was further analyzed and visualized using the cBio Portal[41].

For the IMPACT assay, library construction and sequencing was performed by the MSKCC genomic core facility. Alignment, SNV, and indel calls were performed as described above. Copy number analysis was performed as previously described[13].

SNP6.0 array and analysis

500ng of DNA from each tumor or normal tissue sample was hybridized to the Affymetrix SNP 6.0 arrays using protocols at the Genomic Core Laboratory at MSKCC. Allele-specific copy number for each tumor-normal pair of arrays was calculated using TumorBoost[42] in the Aroma package.

Histology and immunohistochemistry

Tissue processing, embedding, sectioning, and H&E staining was performed by the MSKCC pathology department. Photographs were taken using an Olympus DP21 camera. Immunohistochemistry was performed on archival formalin-fixed, paraffin-embedded tumors using a standard multimer/DAB detection protocol on a Discovery Ultra system (Ventana Medical Systems) with appropriate negative and positive controls. For H3K27me3 staining, we diluted an anti-trimethyl-Histone H3 (Lys27) antibody (#07-449, Millipore) 1:250 in SignalStain Antibody Diluent (#8112, Cell Signaling).

Cell lines and *in vitro* analysis

MPNST724 and ST88-14 human MPNST cell lines were obtained from Jonathan A. Fletcher laboratory at DFCI and have been tested mycoplasma free. MPNST 724 was grown in RPMI with 10% FBS and ST88-14 was grown in RPMI with 15% FBS. cDNA for wild-type human EED and SUZ12 in pDONR vectors were obtained from Harvard PlasmidID

and cloned into MSCV-based retroviral vector with FLAG-HA (FH) tag (Addgene plasmid 41033)[43] using Gateway technology. To generate stably expressing cell lines, MPNST724 and ST88-14 were infected with empty vector, MSCV-FH-EED, MSCV-FH-SUZ12 and selected using puromycin (2 μg/ml for 72 hours). Growth curve of the infected cells was performed using Alamar blue cell viability reagent (Life Technology, DAL1100).

For immunofluorescence of infected cell lines, cells were fixed in 4% paraformaldehyde for 10 minutes, permeabilized in 0.1% Triton X-100, and blocked for 1 hours using 10% goat serum. The cells were then incubated for 2 hours in primary antibody (H3K27me3, #9733, Cell Signaling, 1:400) followed by secondary antibody (Alexa-594 conjugated goat-anti-rabbit, Invitrogen). Slides were mounted using Prolong Gold with DAPI (Invitrogen). Photographs were taken on a Nikon microscopy using a Roeper Scientific camera.

Western blotting

Cell lysates were prepared in RIPA buffer (#9806, Cell Signaling) supplemented with Halt protease and phosphatase inhibitor cocktail (#78440, Thermo Scientific). Equal amounts of protein, as measured by BCA protein assay (#23225, Thermo Scientific), were resolved in NuPAGE® Novex® 4–12% Bis-Tris Protein Gels (#NP0321BOX, Life Technologies) and transferred electrophoretically onto a Nitrocellulose 0.45 μm membrane (#162-0115, BioRad). Membranes were blocked for 1 hour at room temperature in 5% BSA in TBST before being incubated overnight at 4°C with the primary antibodies diluted at 1:1000 in 5% BSA in TBST. NF1 (#sc-67, Santa Cruz, 1:500), EZH1 (#ab13665, Abcam, 1:1000), EZH2 (#5246, Cell signaling,1:1000), SUZ12 (#3737, Cell Signaling, 1:1000), EED (#ab4469, Abcam, 1:1000), H3K27me3 (#9733, Cell Signaling, 1:1000), H3K27Ac (#ab4729, Abcam, 1:1000), HRP-conjugated Total H3 (#12648, Cell Signaling, 1:1000), and HRP-conjugated Actin(#ab49900, Abcam, 1:5000) antibodies were used.

Choromatin immunoprecipitation (ChIP)-qPCR

Chromatin isolation from MPNST724 and ST88-14 cells with different experimental conditions was performed as previously described[44]. For SUZ12 re-expression with associated vector control (Flag-HA-tagged-beta glucuronidase (GUS)), chromatin was isolated approximately 2 weeks after lentiviral infection. EZH2 (#5246, Cell signaling), SUZ12 (#3737, Cell Signaling), H3K27me3 (#9733, Cell Signaling), H3K27Ac (#ab4729, Abcam), H3K4me3 (#39159, Active Motif) antibodies were used for ChIP. The human ChIP-qPCR primer pairs sequences are in Supplementary Table 8.

RNA isolation and qRT-PCR

For tissue culture cells, RNA was isolated using E.Z.N.A. total RNA kit (Omega). For qRT-PCR, RNA was reverse transcribed using High-Capacity cDNA Reverse Transcription Kit (ABI) and PCR was run using Power SYBR Master Mix (ABI) on a Realplex machine (Eppendorf). Expression was normalized to the ribosomal protein RPL27. The primer pairs used are listed in Supplementary Table 8.

Statistical analysis

Fleiss' kappa statistic was used to assess the strength of co-occurrence between *NF1* mutation, *PRC2* mutation, and *CDKN2A* mutation. R package irr was used to calculated the statistic and the *p* value [14].

Supplementary Material

Refer to Web version on PubMed Central for supplementary material.

Acknowledgments

Next generation sequencing and SNP6.0 was done at the Memorial Sloan-Kettering Cancer Center (MSKCC) Genomics Core Facility, Center for Molecular Oncology (CMO). The authors thank members of the cBio Portal team, Jianjiong Gao, Benjamin Gross, Nikolaus Schultz and Chris Sander, for assistance with data analysis and visualization. The authors also thank Timothy Chan, Human Oncology and Pathogenesis Program (HOPP), MSKCC, and the HOPP informatics for assistance with data analysis. This work was supported in part by grants from the NIH for W. L. (NCI U24-CA143840), the Harry J. Lloyd Trust - Translational Research Grant to T.W., the Charles H. Revson Senior Fellowship to T.W., the Jubilaeumsfonds of the Oesterreichische Nationalbank to T.W.; the NIH to P.C. (P50CA140146, CDA; DP2CA174499; K08CA151660), the NIH to Y.C. (K08CA140946), the NIH to LXQ (P50CA140146), the NIH to C.R.A (P50CA140146), the NIH to S.S. (P50CA140146), the Sidney Kimmel Foundation to P.C. (Kimmel Scholar Award), the Cycle for Survival Fund to P. C..

References

1. Brennan, MF.; Antonescu, CR.; Maki, RG. Management of Soft Tissue Sarcoma. Springer; New York: 2013. p. 553
2. LaFemina J, et al. Oncologic outcomes of sporadic, neurofibromatosis-associated, and radiation-induced malignant peripheral nerve sheath tumors. Ann Surg Oncol. 2013; 20:66–72. [PubMed: 22878618]
3. Stucky CC, et al. Malignant peripheral nerve sheath tumors (MPNST): the Mayo Clinic experience. Ann Surg Oncol. 2012; 19:878–85. [PubMed: 21861229]
4. Eilber FC, et al. Validation of the postoperative nomogram for 12-year sarcoma-specific mortality. Cancer. 2004; 101:2270–5. [PubMed: 15484214]
5. Rodriguez FJ. Peripheral nerve sheath tumors: the elegant chapter in surgical neuropathology. Acta Neuropathol. 2012; 123:293–4. [PubMed: 22311741]
6. Antonescu, CR.; Scheithauer, BW.; Woodruff, JM. Tumors of the Peripheral Nervous System. The American Registry of Pathology; Silver Spring, Maryland: 2013. p. 553
7. Taylor BS, et al. Advances in sarcoma genomics and new therapeutic targets. Nat Rev Cancer. 2011; 11:541–57. [PubMed: 21753790]
8. Margueron R, Reinberg D. The Polycomb complex PRC2 and its mark in life. Nature. 2011; 469:343–9. [PubMed: 21248841]
9. Kourea HP, Orlow I, Scheithauer BW, Cordon-Cardo C, Woodruff JM. Deletions of the INK4A gene occur in malignant peripheral nerve sheath tumors but not in neurofibromas. Am J Pathol. 1999; 155:1855–60. [PubMed: 10595915]
10. Menon AG, et al. Chromosome 17p deletions and p53 gene mutations associated with the formation of malignant neurofibrosarcomas in von Recklinghausen neurofibromatosis. Proc Natl Acad Sci U S A. 1990; 87:5435–9. [PubMed: 2142531]
11. Nielsen GP, et al. Malignant transformation of neurofibromas in neurofibromatosis 1 is associated with CDKN2A/p16 inactivation. Am J Pathol. 1999; 155:1879–84. [PubMed: 10595918]
12. Perrone F, et al. p15INK4b, p14ARF, and p16INK4a inactivation in sporadic and neurofibromatosis type 1-related malignant peripheral nerve sheath tumors. Clin Cancer Res. 2003; 9:4132–8. [PubMed: 14519636]

13. Won HH, Scott SN, Brannon AR, Shah RH, Berger MF. Detecting somatic genetic alterations in tumor specimens by exon capture and massively parallel sequencing. J Vis Exp. 2013:e50710. [PubMed: 24192750]
14. Fleiss JL. Measuring nominal scale agreement among many raters. Psychological Bulletin. 1971; 76(5):378–382.
15. Kim J, et al. A Myc network accounts for similarities between embryonic stem and cancer cell transcription programs. Cell. 2010; 143:313–24. [PubMed: 20946988]
16. Mikkelsen TS, et al. Genome-wide maps of chromatin state in pluripotent and lineage-committed cells. Nature. 2007; 448:553–60. [PubMed: 17603471]
17. Meissner A, et al. Genome-scale DNA methylation maps of pluripotent and differentiated cells. Nature. 2008; 454:766–70. [PubMed: 18600261]
18. Andor N, Harness JV, Muller S, Mewes HW, Petritsch C. EXPANDS: expanding ploidy and allele frequency on nested subpopulations. Bioinformatics. 2014; 30:50–60. [PubMed: 24177718]
19. Varambally S, et al. The polycomb group protein EZH2 is involved in progression of prostate cancer. Nature. 2002; 419:624–9. [PubMed: 12374981]
20. Simon JA, Lange CA. Roles of the EZH2 histone methyltransferase in cancer epigenetics. Mutat Res. 2008; 647:21–9. [PubMed: 18723033]
21. Morin RD, et al. Somatic mutations altering EZH2 (Tyr641) in follicular and diffuse large B-cell lymphomas of germinal-center origin. Nat Genet. 2010; 42:181–5. [PubMed: 20081860]
22. Ernst T, et al. Inactivating mutations of the histone methyltransferase gene EZH2 in myeloid disorders. Nat Genet. 2010; 42:722–6. [PubMed: 20601953]
23. Nikoloski G, et al. Somatic mutations of the histone methyltransferase gene EZH2 in myelodysplastic syndromes. Nat Genet. 2010; 42:665–7. [PubMed: 20601954]
24. Ntziachristos P, et al. Genetic inactivation of the polycomb repressive complex 2 in T cell acute lymphoblastic leukemia. Nat Med. 2012; 18:298–301. [PubMed: 22237151]
25. Zhang J, et al. The genetic basis of early T-cell precursor acute lymphoblastic leukaemia. Nature. 2012; 481:157–63. [PubMed: 22237106]
26. Ezhkova E, et al. EZH1 and EZH2 cogovern histone H3K27 trimethylation and are essential for hair follicle homeostasis and wound repair. Genes Dev. 2011; 25:485–98. [PubMed: 21317239]
27. Shen X, et al. EZH1 mediates methylation on histone H3 lysine 27 and complements EZH2 in maintaining stem cell identity and executing pluripotency. Molecular cell. 2008; 32:491–502. [PubMed: 19026780]
28. Xie H, et al. Polycomb repressive complex 2 regulates normal hematopoietic stem cell function in a developmental-stage-specific manner. Cell Stem Cell. 2014; 14:68–80. [PubMed: 24239285]
29. Margueron R, et al. Ezh1 and Ezh2 maintain repressive chromatin through different mechanisms. Molecular cell. 2008; 32:503–18. [PubMed: 19026781]
30. Dobin A, et al. STAR: ultrafast universal RNA-seq aligner. Bioinformatics. 2013; 29:15–21. [PubMed: 23104886]
31. Anders S, Pyl PT, Huber W. HTSeq – A Python framework to work with high-throughput sequencing data. bioRxiv. 2014
32. Anders S, Huber W. Differential expression analysis for sequence count data. Genome Biol. 2010; 11:R106. [PubMed: 20979621]
33. Huang da W, Sherman BT, Lempicki RA. Systematic and integrative analysis of large gene lists using DAVID bioinformatics resources. Nat Protoc. 2009; 4:44–57. [PubMed: 19131956]
34. Subramanian A, et al. Gene set enrichment analysis: a knowledge-based approach for interpreting genome-wide expression profiles. Proc Natl Acad Sci U S A. 2005; 102:15545–50. [PubMed: 16199517]
35. Li H, Durbin R. Fast and accurate long-read alignment with Burrows-Wheeler transform. Bioinformatics. 2010; 26:589–95. [PubMed: 20080505]
36. McKenna A, et al. The Genome Analysis Toolkit: a MapReduce framework for nalyzing next-generation DNA sequencing data. Genome Res. 2010; 20:1297–303. [PubMed: 20644199]
37. Cibulskis K, et al. Sensitive detection of somatic point mutations in impure and heterogeneous cancer samples. Nat Biotechnol. 2013; 31:213–9. [PubMed: 23396013]

38. Saunders CT, et al. Strelka: accurate somatic small-variant calling from sequenced tumor-normal sample pairs. Bioinformatics. 2012; 28:1811–7. [PubMed: 22581179]
39. Koboldt DC, et al. VarScan 2: somatic mutation and copy number alteration discovery in cancer by exome sequencing. Genome Res. 2012; 22:568–76. [PubMed: 22300766]
40. Forbes SA, et al. The Catalogue of Somatic Mutations in Cancer (COSMIC). Curr Protoc Hum Genet. 2008; Chapter 10(Unit 10):11. [PubMed: 18428421]
41. Cerami E, et al. The cBio cancer genomics portal: an open platform for exploring multidimensional cancer genomics data. Cancer Discov. 2012; 2:401–4. [PubMed: 22588877]
42. Bengtsson H, Neuvial P, Speed TP. TumorBoost: normalization of allele-specific tumor copy numbers from a single pair of tumor-normal genotyping microarrays. BMC Bioinformatics. 2010; 11:245. [PubMed: 20462408]
43. Sowa ME, Bennett EJ, Gygi SP, Harper JW. Defining the human deubiquitinating enzyme interaction landscape. Cell. 2009; 138:389–403. [PubMed: 19615732]
44. Chi P, et al. ETV1 is a lineage survival factor that cooperates with KIT in gastrointestinal stromal tumours. Nature. 2010; 467:849–53. [PubMed: 20927104]

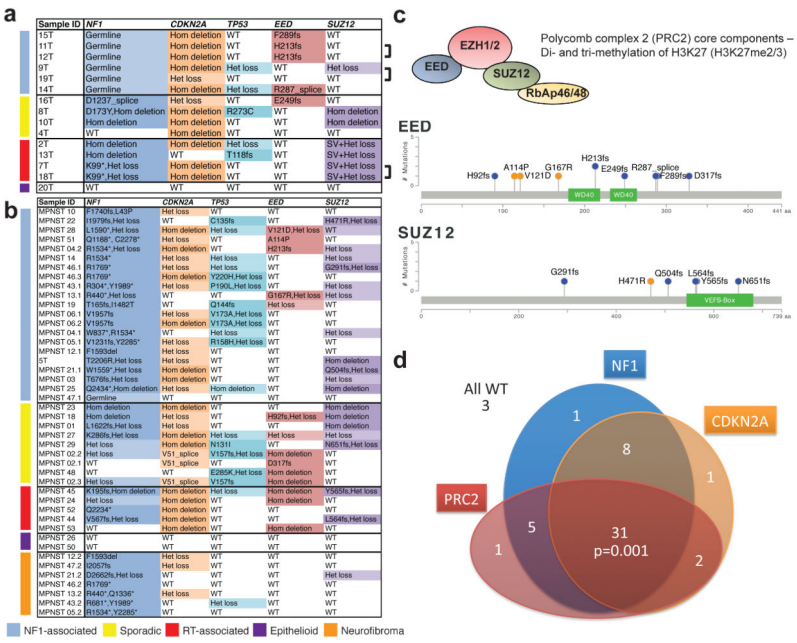

Figure 1. Most frequent genetic alterations in MPNSTs (NF1-associated, sporadic, radiotherapy-associated and epithelioid) and neurofibromas

(**a, b)** Non-synonymous single nucleotide variants (SNVs) and copy number variants (CNVs) in 15 MPNSTs with matched normal pairs by WES, SNP6.0 and RNA-seq (**a**), and in 37 MPNSTs and 7 neurofibromas by targeted sequencing (IMPACT) (**b**). Bracket indicates two different tumor samples from the same patient. (**c**) Schematics of the non-synonymous SNVs observed in the PRC2 core components, *EED* and *SUZ12*, in 15 WES and 37 custom IMPACT MPNST samples. (**d**) Schematic of the overlap of mutations affecting *NF1*, PRC2 components (*EED* or *SUZ12*) and *CDKN2A* in all MPNSTs (NF1-associated, sporadic, radiotherapy-associated and epithelioid). Fleiss' Kappa statistics, 3 way comparison of *NF1*, *CDKN2A* and PRC2 (*EED* or *SUZ12*) genetic alteration suggested that they significantly co-occur, Kappa= 0.21, *p=0.001*.

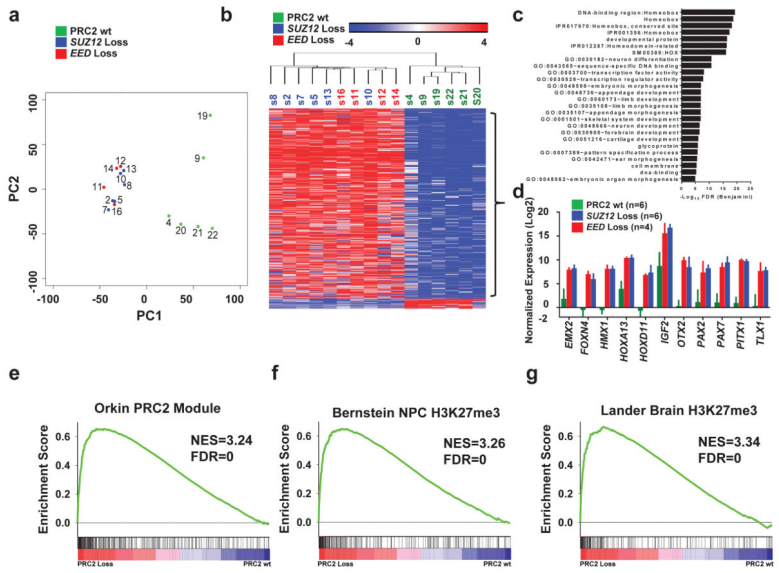

Figure 2. PRC2–loss MPNSTs exhibit distinct gene expression pattern from PRC2 wild-type MPNSTs, signifying activation of developmentally suppressed pathways

(a) Principal component analysis of the MPNST whole-transcriptome revealed that the PRC2 wild-type (wt) and PRC2-loss (*SUZ12* loss and *EED* loss) samples segregate by principal component 1 (PC1). Each sample is color coded based on their corresponding PRC2 mutational status derived from WES except for S21 and S22 which are based on manual examination of the RNA-seq for mutations in the PRC2 components. Green: PRC2 wt; blue: *SUZ12* loss; red: *EED* loss. (**b**) Heatmap of significantly differentially expressed genes between PRC2-loss and PRC2-wt MPNSTs identified by RNA-seq. Clustering was based on most differentially expressed 479 genes with FDR <0.05 and fold-change >8.0 (Supplementary Table 2). Samples are color coded based on PRC2 mutational status, green: PRC2 wt; blue: *SUZ12* loss; red: *EED* loss. Scale bar, mean normalized fold change by log2. (**c**) Gene Ontology analysis of the differentially upregulated genes in PRC2-losscompared to PRC2-wt MPNSTs. (**d**) Gene expression by RNA-seq of a representative group of developmental master regulators and imprinted genes in PRC2-loss and PRC2-wt MPNSTs. Error bars +s.e.m. (**e–g**) GSEA plots of the ranked list of the differentially expressed genes between PRC2-loss and PRC2-wt MPNSTs using three gene sets: PRC2 module (**e**), the H3K27me3 targets in brain (**g**) and neural precursor cells (**f**).

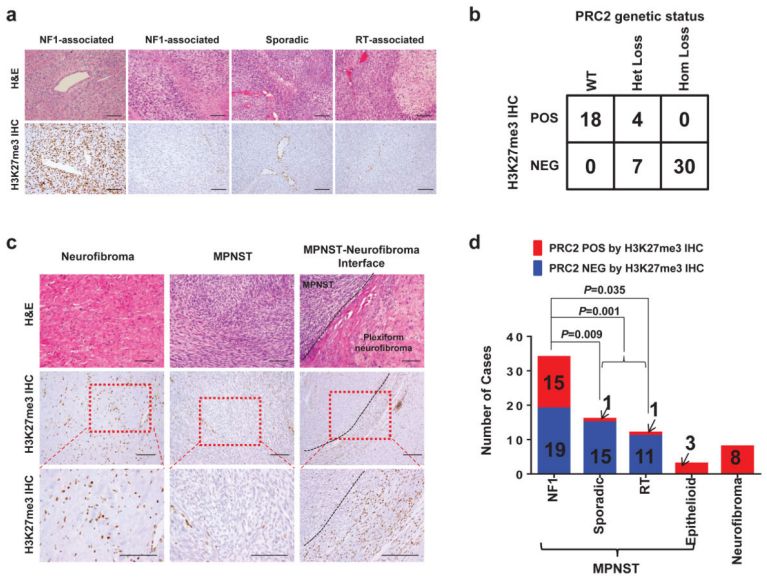

Figure 3. H3K27me3 IHC significantly correlates with PRC2 genetic status and H3K27me3 loss characterizes progression from neurofibroma to MPNST

(a) Representative H&E and H3K37me3 IHC images of NF1-associated, sporadic and radiotherapy associated MPNSTs. Scale bars: 100 μm. (**b**) Correlation of PRC2 genetic status by WES, RNA-seq and custom targeted sequencing and H3K27me3 IHC status. (**c**) Representative H&E and H3K27me3 IHC images of neurofibroma, NF1-associated MPNST, and the interface of plexiform neurofibroma transition into MPNST. (**d**) Distribution of PRC2 loss (blue) and PRC2 presence (red) by H3K27me3 IHC in NF1-associated, sporadic, radiotherapy-associated, and epithelioid MPNSTs, and neurofibromas. Fisher's exact test was used to calculate the *p* value.

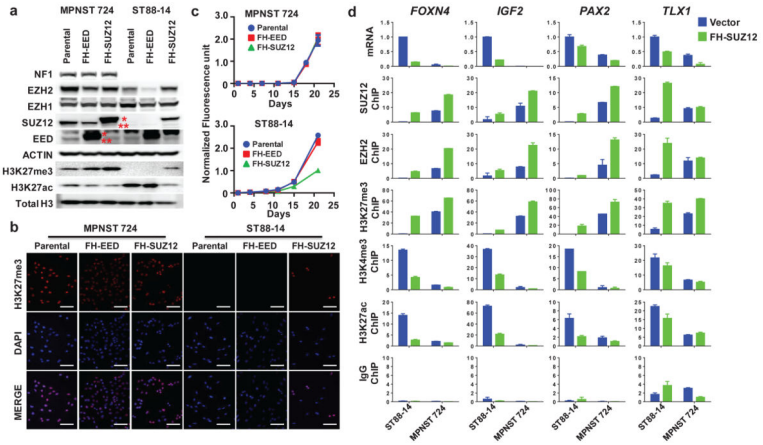

Figure 4. PRC2 loss promotes cell proliferation and growth in PRC2-loss MPNST

(**a**) Immunoblots demonstrating SUZ12 loss and corresponding loss of H3K27me3 in ST88-14, a NF1-associated human MPNST cell line compared to a sporadic human MPNST cell line, MPNST724, with intact PRC2 and retained H3K27me3 expression. Introduction of exogenous Flag-HA-tagged SUZ12 (FH-SUZ12), but not Flag-HA-tagged EED (FH-EED) in ST88-14 restores the H3K27me3 protein levels. *: exogenous Flag-HA-tagged SUZ12 or EED; **: endogenous SUZ12 or EED. (**b**) Immunofluorescence (IF) of H3k27me3 demonstrating the restoration of H3K27me3 at the cellular level by introducing FH-SUZ12 in ST88-14 MPNST cell line with SUZ12 loss. Scale bars: 100 μm. (**c**) Representative growth curves of MPNST724 and ST88-14 demonstrating that introduction of FH-SUZ12, but not FH-EED, in the *SUZ12*-deficient ST88-14 cells leads to significant growth retardation, whereas it had no effect in MPNST724 cells. Similar results have been obtained in at least 3 independent experiments. (**d**) ST88-14 and MPNST724 cells were infected with vector control (blue) and FH-SUZ12 (green). Plots of the qRT-PCR expression (expressed as $2^{-\Delta\Delta Ct}$) and ChIP-qPCR promoter localization (expressed as % input) of SUZ12, EZH2, H3K27me3, H3K4me3, H3K27ac, and IgG control of *FOXN4*, *IGF2*, *PAX2*, and *TLX1* genes are shown. Error bars +s.e.m. n=3.